

JGR Space Physics



RESEARCH ARTICLE

10.1029/2020JA028560

A Case Study of Transversely Heated Low-Energy Helium Ions by EMIC Waves in the Plasmasphere

Khan-Hyuk Kim¹ , Hyuck-Jin Kwon² , Junhyun Lee¹, Ho Jin¹, and Jungjoon Seough³

¹School of Space Research, Kyung Hee University, Gyeonggi, South Korea, ²Division of Climate Change Research, Korea Polar Research Institute, Incheon, South Korea, ³Korea Astronomy and Space Science Institute, Daejeon, South Korea

Key Points:

- EMIC wave activity is clearly correlated with low-energy (<10 eV) He⁺ flux enhancement
- The low-energy He⁺ ions are transversely heated by EMIC waves
- EMIC waves strongly affect the low-energy He⁺ ions rather than the low-energy H⁺ ions

Correspondence to:

K.-H. Kim,
khan@khu.ac.kr

Citation:

Kim, K.-H., Kwon, H.-J., Lee, J., Jin, H., & Seough, J. (2021). A case study of transversely heated low-energy helium ions by EMIC waves in the plasmasphere. *Journal of Geophysical Research: Space Physics*, 126, e2020JA028560. <https://doi.org/10.1029/2020JA028560>

Received 5 AUG 2020
 Accepted 16 JAN 2021

Abstract The Van Allen Probe A spacecraft observed strong ~0.5-Hz helium (He⁺) band and weak ~0.8-Hz hydrogen (H⁺) band EMIC waves on April 17, 2018, at $L = \sim 4.5\text{--}5.2$, in the dawn sector, near the magnetic equator, and close to the plasmapause. We examined low-energy ion fluxes observed by the Helium Oxygen Proton and Electron (HOPE) instrument onboard Van Allen Probe A during the wave interval and found that low-energy He⁺ flux (<10 eV) enhancements occur nearly simultaneously with He-band and H-band EMIC wave power enhancements in a direction mostly perpendicular to the background magnetic field without significant low-energy H⁺ and O⁺ flux variations. We suggest that cold He⁺ ions (<1 eV) are preferentially and transversely heated up 10 eV through the interaction with EMIC waves inside the plasmasphere. The low-Earth orbit spacecraft observed localized precipitations of energetic protons in the upper ionosphere at subauroral latitudes near the magnetic field footprint of Van Allen Probe A. Our observations provide a clear evidence that EMIC waves play an important role in the overall dynamics in the inner magnetosphere, contributing to the high-energy particle loss and low-energy particle energization.

1. Introduction

Early theoretical works described that electromagnetic ion cyclotron (EMIC) waves are generated as transverse left-handed polarized waves near the magnetic equator by anisotropic ($T_{\perp} > T_{\parallel}$) protons with energies of ~10–100 keV, which are typical ion energies in the ring current (e.g., Cornwall, 1965; Kennel & Petschek, 1966). EMIC waves are excited during geomagnetically disturbed intervals associated with geomagnetic storms, substorms, and solar wind dynamic pressure variations (e.g., Fraser & McPheron, 1982; Ishida et al., 1987; K.-H. Kim et al., 2017; Meredith et al., 2003; Ol'son & Lee, 1983; Usanova et al., 2008) and also occur under quiet geomagnetic conditions (K.-H. Kim et al., 2016a; Park et al., 2016) over a wide L range (~4–12) at all local times in the Earth's magnetosphere (e.g., Allen et al., 2015; Anderson et al., 1992a, 1992b; Fraser & Nguyen, 2001; Keika et al., 2013; G.-J. Kim et al., 2016; Min et al., 2012; Saikin et al., 2015; Usanova et al., 2012). The frequency of EMIC waves observed in the magnetosphere falls in the Pc1-Pc2 geomagnetic pulsation band (frequency = ~0.1–5 Hz). Ground magnetometers located at low to high latitudes routinely detect geomagnetic pulsations in the Pc1-Pc2 band (e.g., Bortnik et al., 2008; Engebretson et al., 2002; Kwon et al., 2020; Mann et al., 2014; Nomura et al., 2011). These ground Pc1-Pc2 pulsations have been attributed to EMIC waves propagating to the ground through the ionosphere along the field lines from the source region in the magnetosphere (e.g., H. Kim et al., 2017; Usanova et al., 2008).

Studies of EMIC waves including cold heavy ions (He⁺ and O⁺) reported that the heavy ions play a significant role in determining the spectral and propagation properties of EMIC waves even though in small concentrations of cold heavy ions (~5%–10% for He⁺ and ~1%–2% for O⁺) (Kozyra et al., 1984; Mauk et al., 1981; Roux et al., 1982; Young et al., 1981). In the presence of such cold heavy ions, EMIC waves can be generated in three distinct bands: a H-band between the local H⁺ gyrofrequency (f_{H^+}) and He⁺ gyrofrequency (f_{He^+}), a He-band between the local He⁺ gyrofrequency (f_{He^+}) and O⁺ gyrofrequency (f_{O^+}), and an O-band below f_{O^+} . In situ observations in the inner and outer magnetosphere have provided clear evidence for the cold heavy ion effects. Statistical studies of EMIC waves using AMPTE/CCE and THEMIS data showed that the He-band occurrence rate is high in the late afternoon at $L = \sim 9$ and that the occurrence rate of H-band

© 2021. The Authors.

This is an open access article under the terms of the Creative Commons Attribution License, which permits use, distribution and reproduction in any medium, provided the original work is properly cited.

waves is peaked in the dawnside sector at $L = \sim 10\text{--}12$ (Anderson et al., 1992a, 1992b; Keika et al., 2013; G.-J. Kim et al., 2016; Min et al., 2012). Since low frequencies in O-band waves are overlapped with a frequency of background magnetic field oscillations, there are few observations of O-band EMIC waves (e.g., Fraser et al., 1980; Sakaguchi et al., 2013).

EMIC waves interact with energetic protons and relativistic radiation belt electrons. These resonant wave-particle interactions cause pitch angle scattering that leads to subsequent precipitation of energetic protons and relativistic electrons into the atmosphere. The EMIC wave scattering is currently considered one of the leading loss processes of energetic protons and relativistic electrons in the magnetosphere. Theoretical studies of the early 1970s suggested resonant pitch angle scattering of protons and electrons by EMIC waves (Lyons & Thorne, 1972; Thorne & Kennel, 1971). Evidence for EMIC wave-induced scattering has been reported from the observations of polar-orbiting POES and METOP spacecraft in the upper ionosphere (e.g., Bingley et al., 2019; Clilverd et al., 2007; Hendry et al., 2016; Hyun et al., 2014; K.-H. Kim et al., 2016b; Liu et al., 2018; Miyoshi et al., 2008; Rodger et al., 2008; Sandanger et al., 2009; Yuan et al., 2012; Zhang et al., 2016). Simultaneous appearance of isolated proton auroras and Pc1 geomagnetic pulsations at subauroral latitudes provides evidence for wave-particle interactions with EMIC waves generated near the plasmapause (Sakaguchi et al., 2008).

Previous numerical studies suggested that EMIC waves can preferentially heat cold He^+ ions in the direction perpendicular to the ambient magnetic field (e.g., Gendrin & Roux, 1980; Mauk, 1982a, 1982b; Omid et al., 2010; Omura et al., 1985; Qian et al., 1990). Earlier observations at geosynchronous orbit showed the acceleration of cold He^+ ions up to suprathermal energies (tens of eV to a few hundred eV) (Mauk & McPherron, 1980; Roux et al., 1982; Young et al., 1981). AMPTE/CCE observations in the outer magnetosphere ($L \sim 6\text{--}9$) also reported that cold He^+ ions are transversely heated to average temperatures of about 35 eV and sometimes above 100 eV through the interaction with EMIC waves (Anderson & Fuselier, 1994). Zhang et al. (2011) using data from the Cluster spacecraft in the outer magnetosphere ($L \sim 8\text{--}14$) showed that the He^+ ions resonantly interacted with EMIC waves and were perpendicularly energized to energies up to 1 keV. Although the EMIC wave-associated He^+ ion heating has been reported using the data obtained in the outer magnetosphere, there are few spacecraft observations for cold He^+ ion heating by EMIC waves in the inner magnetosphere ($L < 6$) (Yuan et al., 2016).

In this study, we have analyzed magnetic field and low-energy particles data acquired by the Radiation Belt Storm Probes-A spacecraft from $L = \sim 4.5\text{--}5.2$. We observed EMIC waves just inside the plasmapause near the magnetic equator and a clear correlation between the EMIC wave activity and low-energy (<10 eV) He^+ flux enhancement. We suggest that cold He^+ ions are heated up to 10 eV through the interaction with EMIC waves and discuss which frequency band of EMIC waves contributes to heating the cold He^+ ions in the plasmasphere. Using the magnetic field and energetic proton data obtained from the low-Earth orbit spacecraft in the upper ionosphere, we also show localized precipitation of energetic protons occurring near the magnetic footprint of the EMIC wave's source region.

2. Data Sets

In this study, we use the magnetometer data (64 samples per second) obtained by EMFISIS (Electric and Magnetic Field Instrument Suite and Integrated Science) instrument package (Kletzing et al., 2013) onboard the Van Allen Probe A to examine the properties of EMIC waves observed on April 17, 2018. The Van Allen Probe A magnetic field data are exactly resampled at 0.1 s intervals after interpolation and presented in a mean-field-aligned (MFA) coordinate system. In this system, $\hat{\mathbf{e}}_z$ is in the direction of the mean magnetic field, which is defined by taking 5 min boxcar running averages of the 0.1 s data; $\hat{\mathbf{e}}_y$ (eastward) is parallel to $\hat{\mathbf{e}}_z \times \mathbf{r}$, where \mathbf{r} is the radial vector pointing from the center of the Earth toward the spacecraft; and $\hat{\mathbf{e}}_x$ (radially outward) is given by $\hat{\mathbf{e}}_x = \hat{\mathbf{e}}_y \times \hat{\mathbf{e}}_z$. To be consistent, the perturbed parallel magnetic field component (δB_z) is defined by B_z (0.1 s averages) minus B_z (5 min averages). The EMFISIS experiment includes a plasma wave spectrum analyzer, which provides information on the electron number density (Kurth et al., 2015). We have used the electron density to identify the plasmapause location. The Van Allen Probe A particle data used in this study include low-energy (<52 keV) ion fluxes measured by the Helium Oxygen Proton Electron (HOPE) instrument (Funsten et al., 2013). We also use the NOAA-15 spacecraft observations from

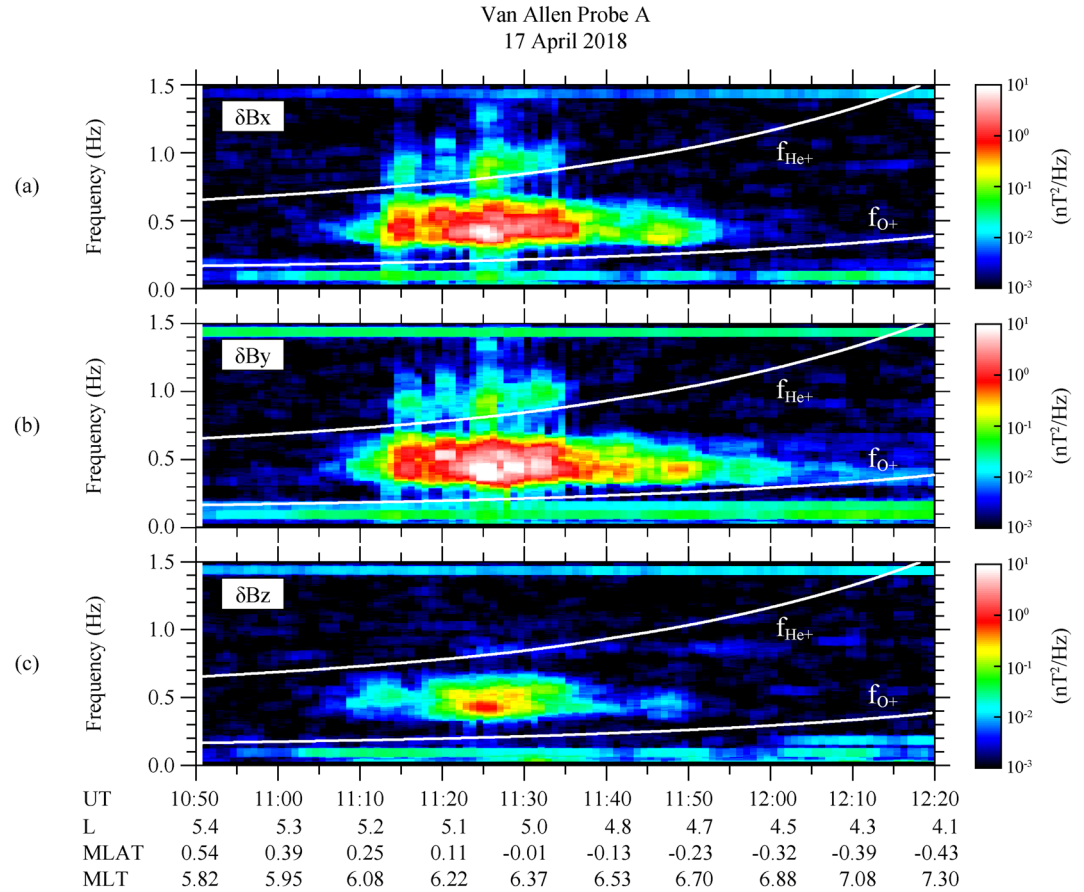


Figure 1. Dynamic spectra of the transverse components, (a) δB_x and (b) δB_y , and compressional component (c) δB_z in a mean-field-aligned coordinate system at Van Allen Probe A for the interval from 10:50 to 12:20 UT on April 17, 2018. Two white lines indicate the local helium (f_{He^+}) and oxygen (f_{O^+}) gyrofrequencies.

the Medium Energy Proton and Electron Detector (MEPED) (Evans & Greer, 2004) in Sun-synchronous near-polar orbits at ~ 850 km altitude to examine the precipitating energetic protons into atmosphere due to pitch angle scattering associated with EMIC waves.

3. Observations

3.1. EMIC Wave Observations in the Inner Magnetosphere

Figures 1a–1c show the magnetic field dynamic spectra of the transverse (δB_x and δB_y) and compressional (δB_z) field components of Van Allen Probe A from 10:50 UT to 12:20 UT on April 17, 2018. The spacecraft positions (the magnetic shell parameter L , magnetic local time [MLT], and magnetic latitude [MLAT]) are shown at the bottom using a centered dipole. During the time period Van Allen Probe A was very close to the magnetic equator ($|\text{MLAT}| \leq \sim 0.5^\circ$) on the inbound leg, moving from $L = 5.4$ to $L = 4.1$, within a few hours of local dawn (MLT = 5.8–7.3 h). In the inner magnetosphere ($L < 6$) near the dawnside magnetic equator, Van Allen Probe A observed wave activity in all field components, but strong spectral intensity appears in the transverse δB_x and δB_y components in the frequency band between the local helium (f_{He^+}) and oxygen (f_{O^+}) gyrofrequencies (i.e., He-band) for the interval of $\sim 11:10$ – $11:55$ UT. The compressional δB_z component also exhibits a spectral enhancement in the He-band but with much lower spectral intensity. Van Allen Probe A also observed weak wave activity in the H-band above f_{He^+} in the both transverse components from 11:15 to 11:35 UT.

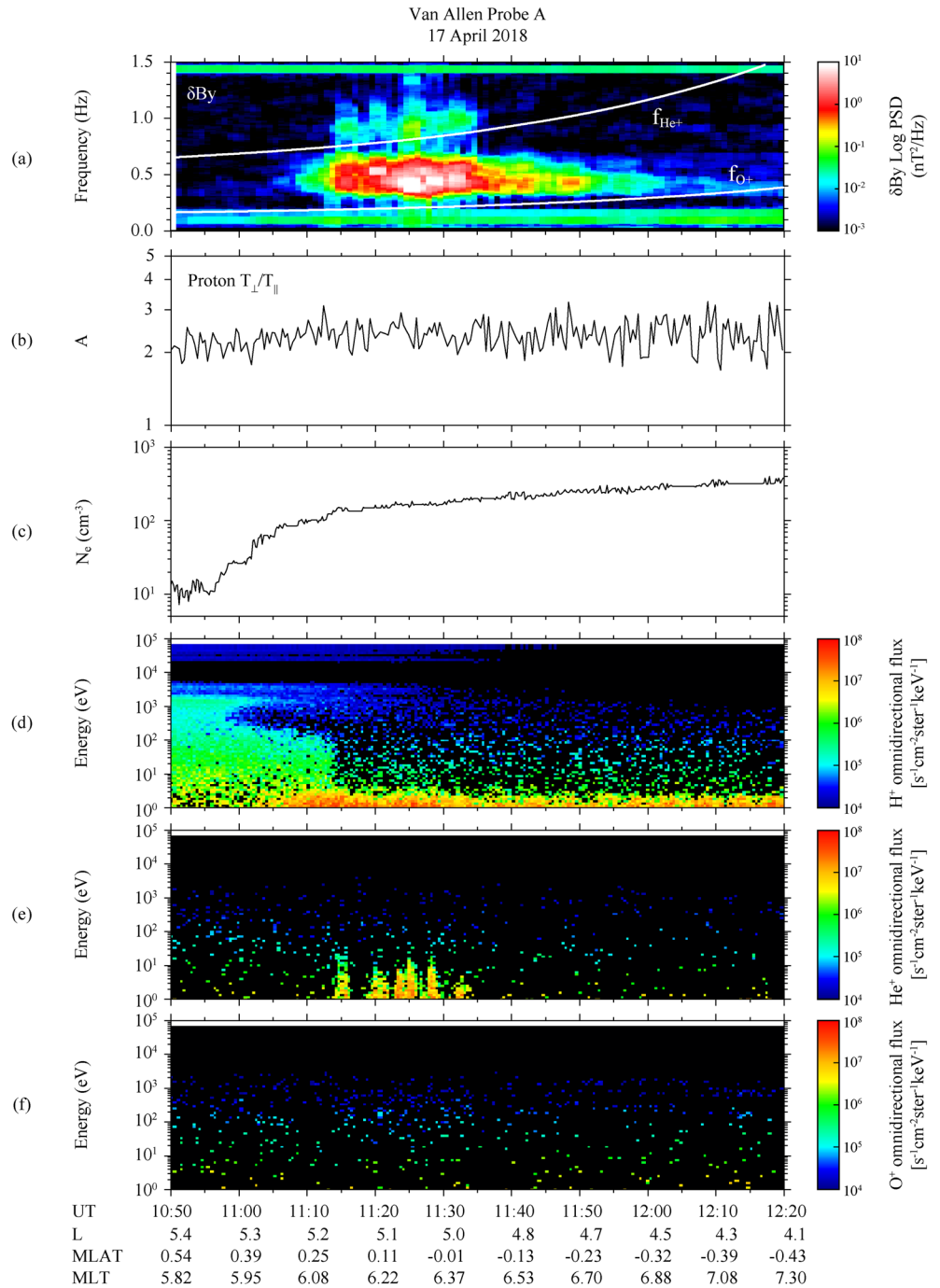


Figure 2. (a) δB_y dynamic spectra. (b) The plasma anisotropies T_{\perp}/T_{\parallel} for protons in the energy range of ~ 10 – 30 keV. (c) Electron number density estimated from the upper hybrid resonance frequency. (d–f) Energy-time spectrograms of the omnidirectional differential fluxes of H^+ , He^+ , and O^+ ions, respectively, measured by the HOPE instrument. HOPE, Helium Proton and Electron.

3.2. Low-Energy He^+ Flux Enhancement During the EMIC Wave Event

Figure 2 shows the δB_y dynamic spectra and local plasma conditions observed at Van Allen Probe A during the 10:50–12:20 interval seen in Figure 1. The plasma anisotropy ($A = T_{\perp}/T_{\parallel}$) for protons in the energy range of ~ 10 – 33 keV are plotted in Figure 2b. The temperature anisotropy is about 2–3 for the 10:50–12:20 interval without an enhancement in wave activity. Since enhanced temperature anisotropies provide free energy for

wave generation, the EMIC waves in Figure 2a may be observed during the time of decay phase of EMIC waves rather than growth and saturation phases (e.g., Fu et al., 2016). The anisotropies in Figure 2b were calculated using the definition given by Chen et al. (1998):

$$A \equiv \frac{\int_0^\pi f(\alpha_0) \sin^3 \alpha_0 d\alpha_0}{2 \int_0^\pi f(\alpha_0) \cos^2 \alpha_0 \sin \alpha_0 d\alpha_0} \quad (1)$$

where f is the particle phase space distribution function, and α_0 is equatorial pitch angle of the particle. We used the relationship $J(E, \alpha) = (v^2/m)f(v, \alpha)$, where J is the measured differential proton flux, v is the proton velocity, and m is the proton mass.

In discussing EMIC wave's generation, it is important to determine where the wave's generation location is with respect to the plasmopause because the cold plasma density plays a significant role in determining the spectral properties of EMIC waves (e.g., G.-J. Kim et al., 2016; Kozyra et al., 1984; Summers & Thorne, 2003; Young et al., 1981). Data from the plasma wave experiment on Van Allen Probe A are used to estimate the electron number density (N_e) based on the relationship between the density and characteristic frequencies in the spectrum: the plasma frequency cutoff of continuum radiation and the upper hybrid resonance (Kurth et al., 2015). To infer the location of the plasmopause, we have examined the plasma wave spectra data provided on NASA/GSFC Space Physics Data Facility Coordinated Data Analysis Web (<https://cdaweb.gsfc.nasa.gov>) and found a clear upper hybrid resonance frequency (data not shown here). The electron plasma frequency (f_{pe}) was extracted from the narrow-band emission at the upper hybrid resonance frequency, and the electron number density was calculated from f_{pe} using

$$N_e (\text{cm}^{-3}) = \left(\frac{f_{pe}}{8979.5 \text{Hz}} \right)^2 \quad (2)$$

The corresponding number density N_e is plotted in Figure 2c. N_e indicates that Van Allen Probe A crossed the plasmopause, which is defined to be an electron density change by a factor of 5 or more over an L distance smaller than 0.5 (e.g., Carpenter & Anderson, 1992), around 10:55–11:10 UT on the inbound leg at $L \sim 5.2$ – 5.3 before the onset of EMIC wave activity, representing that wave generation is not associated with crossing the plasmopause and that the EMIC waves are generated just inside the plasmopause.

Figures 2d–2f show the energy-time spectrograms of the omnidirectional differential fluxes of H^+ , He^+ , and O^+ ions measured by the HOPE instrument on Van Allen Probe A. The fluxes of different ion species are plotted in the same range. The HOPE H^+ data show enhanced fluxes of plasma sheet protons (<1 keV) from 10:50 UT to 11:15 UT when the spacecraft encountered the inner edge of the plasmopause. It has been reported that the inner edge of the plasma sheet coincides with the plasmopause location (e.g., Engebretson et al., 2015; Kwon et al., 2015). The HOPE H^+ data also show weak fluxes in the energy range above 1 keV. They exhibit a band structure with two populations, one between 1 and 5 keV and the other between 20 keV and the instrument energy upper limit of 52 keV, and penetrated to the plasmasphere. This structure is similar to ion nose structures, which are a common feature in the inner magnetosphere, reported by Ferradas et al. (2016). The spectrogram of He^+ shows repeatedly enhanced fluxes in the low-energy population below 10 eV from 11:15 UT to 11:35 UT. These low-energy He^+ flux enhancements occur nearly simultaneously with the intense He-band and weak H-band wave activity interval. No enhanced flux was found in the HOPE O^+ data for the interval.

Figure 3 shows the EMIC wave power integrated over the frequency range of 0.8–1.1 Hz for H-band wave and 0.25–0.7 Hz for the He-band wave, the difference between the observed magnetic field magnitude and model magnetic field magnitude (ΔB_T), and He^+ fluxes for pitch angles 72° , 54° , 36° , and 18° . We used the magnetic field model developed by Tsyganenko and Sitnov (2005) (TS05) at the position of Van Allen Probe A. For the input parameters of the model TS05, solar wind dynamic pressure $P_{sw} = 1.0$ nPa, interplanetary magnetic field (IMF) $B_y = 0$ nT, IMF $B_z = 0$ nT, and $Dst = 0$ nT were used. The vertical dashed lines indicate the center of the interval of each He^+ flux enhancement. As expected in Figure 2, the quasiperiodic appearance of low-energy He^+ flux enhancements after 11:10 UT has a clearly associated enhancement in He-band EMIC wave power greater than 10^{-1} nT². There are enhancements in wave power lower than 10^{-1} nT² at 11:41 UT, 11:49 UT, and 11:56 UT. For these low wave power enhancements there is no corresponding

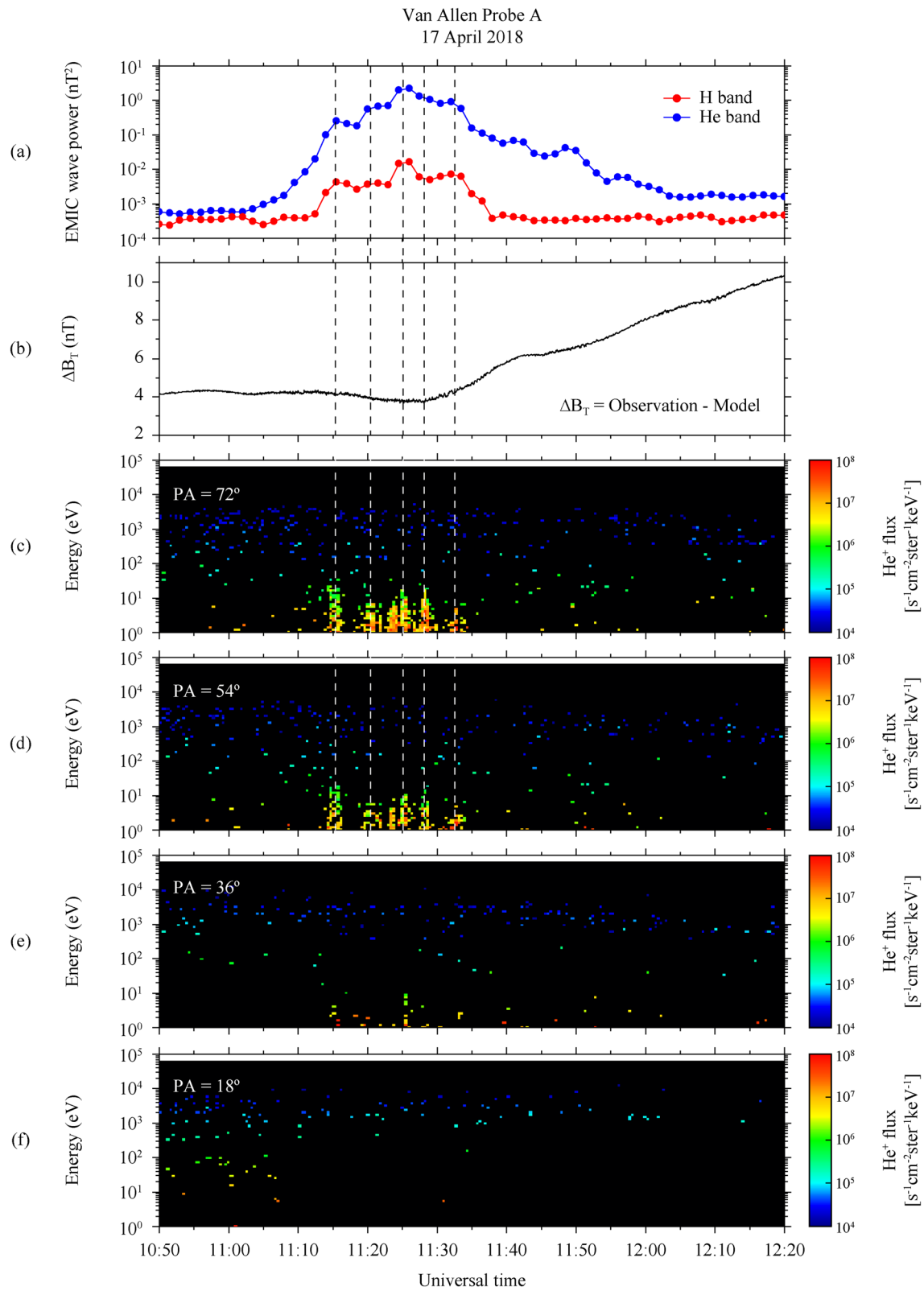


Figure 3. (a) EMIC wave power integrated over the frequency range of 0.8–1.1 Hz for H-band wave and 0.25–0.7 Hz for the He-band wave. (b) Difference between the observed magnetic field magnitude and model magnetic field magnitude. (c–f) He⁺ fluxes for pitch angles 72°, 54°, 36°, and 18°. EMIC, electromagnetic ion cyclotron.

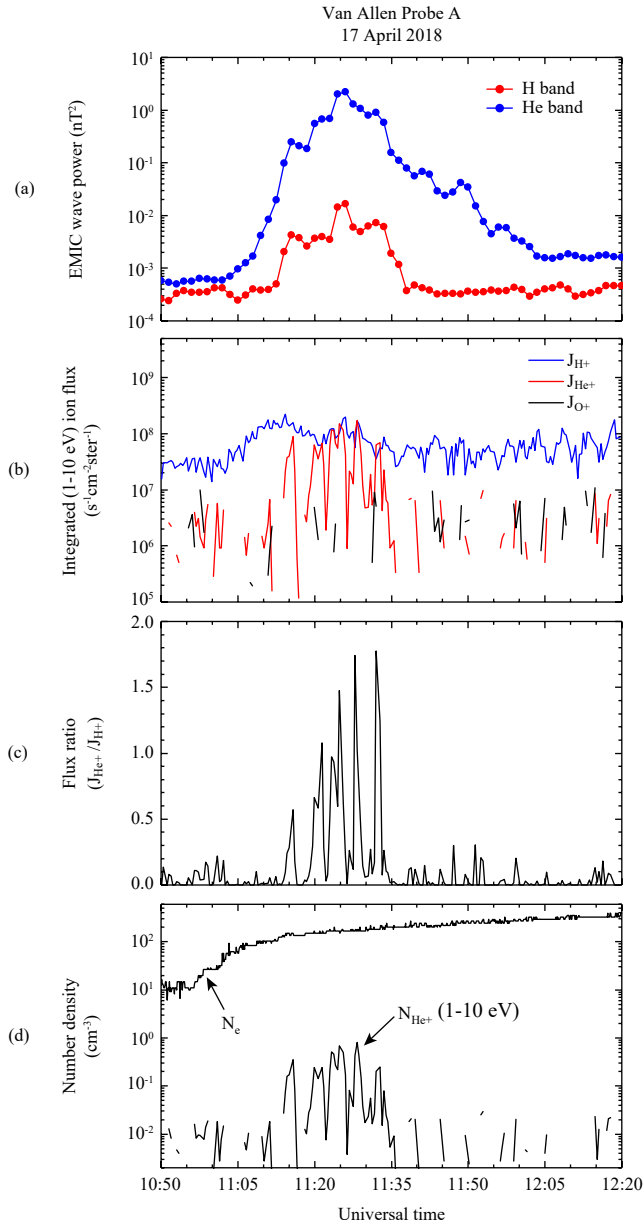


Figure 4. (a) EMIC wave power. (b) Proton (J_{H^+} , blue), helium (J_{He^+} , red), and oxygen (J_{O^+} , black) fluxes summed over the energy range of 1–10 eV. (c) Ratio of J_{He^+} to J_{H^+} . (d) Electron number density N_e obtained from EMFISIS and the number density of low-energy He^+ (N_{He^+}), which is a summation of the density calculated for each energy step from 1 to 10 eV of the HOPE instrument. HOPE, Helium Oxygen Proton and Electron; EMIC, electromagnetic ion cyclotron.

He^+ flux increase. It is likely that lower energy He^+ ion (1–10 eV) enhancements are associated with He-band waves with power greater than 10^{-1} nT^2 . The H-band wave power modulation is also correlated with the He^+ flux enhancement even though its power is much smaller than the He-band wave power. Figures 3c–3f show that the low-energy He^+ flux has no distribution at 18° pitch angle and that the enhanced He^+ flux observed in the EMIC wave interval corresponds to large pitch angle distributions. That is, the flux is mostly enhanced in a direction perpendicular to the magnetic field. ΔB_T is slightly reduced for the interval when the lower energy helium ions appear. The reduced ΔB_T has no time-dependent oscillations corresponding to the flux enhancements. Thus, we suggest that the low-energy He^+ flux enhancement is not driven by long-period external force variations.

Figure 4a repeats the wave power from Figure 3a for easy comparison. Figure 4b shows proton (J_{H^+} , blue), helium (J_{He^+} , red), and oxygen (J_{O^+} , black) fluxes summed over the energy range of 1–10 eV. There are data gaps in J_{He^+} and J_{O^+} . This is due to zero flux intensity of He^+ and O^+ in the energy band. As expected from Figure 2, J_{H^+} is dominant through the time interval of 10:50–12:20 UT, and a gradual increase in J_{H^+} started at $\sim 11:05$ UT when the spacecraft moved into the plasmasphere. Clearly, J_{He^+} exhibits a well-pronounced modulation, corresponding to wave power enhancements, while there is no wave-associated modulation in J_{H^+} and J_{O^+} . To examine the degree of J_{He^+} enhancement relative to J_{H^+} , we have taken the ratio of J_{He^+} to J_{H^+} . The result is shown in Figure 4c. On the basis of the ratio, we find that the helium flux in the low-energy range is more intensified than the proton flux when the strong EMIC waves appear. This indicates that the EMIC waves strongly affect low-energy He^+ ions rather than the H^+ ions. Figure 4d shows the electron number density N_e obtained from EMFISIS and the number density of low-energy He^+ (N_{He^+}), which is a summation of the density calculated for each energy step from 1 to 10 eV of the HOPE instrument using the formula given by Goldstein et al. (2014) and Sarno-Smith et al. (2015):

$$N_{\text{He}^+} = \sum_i 4\pi \sqrt{\frac{m_{\text{He}^+}}{2E_i}} J_i \Delta E_i \quad (3)$$

where the quantity $J_i = J_{\text{He}^+}(E_i)$ is the He^+ differential flux at the median of each energy channel E_i between 1 and 10 eV, ΔE_i is the range of each energy channel, and m_{He^+} is the helium mass. The peak values of N_{He^+} during the enhanced J_{He^+} interval are distributed in the range of $\sim 0.3\text{--}0.8 \text{ cm}^{-3}$ just inside the plasmopause with the local electron number density N_e of $\sim 150\text{--}180 \text{ cm}^{-3}$, representing that N_{He^+} in the energy range of 1–10 eV is $\sim 0.3\text{--}0.5\%$ of the total density.

3.3. NOAA Observations in the Upper Ionosphere

Figures 5b–5d show the differential flux for the 39, 115, and 332-keV proton channels of the precipitating (red) and trapped (blue) particles measured by the Medium Energy Proton and Electron Detector (MEPED) instrument on the low-altitude polar-orbiting NOAA-15 spacecraft. The MLAT and MLT of NOAA-15 and

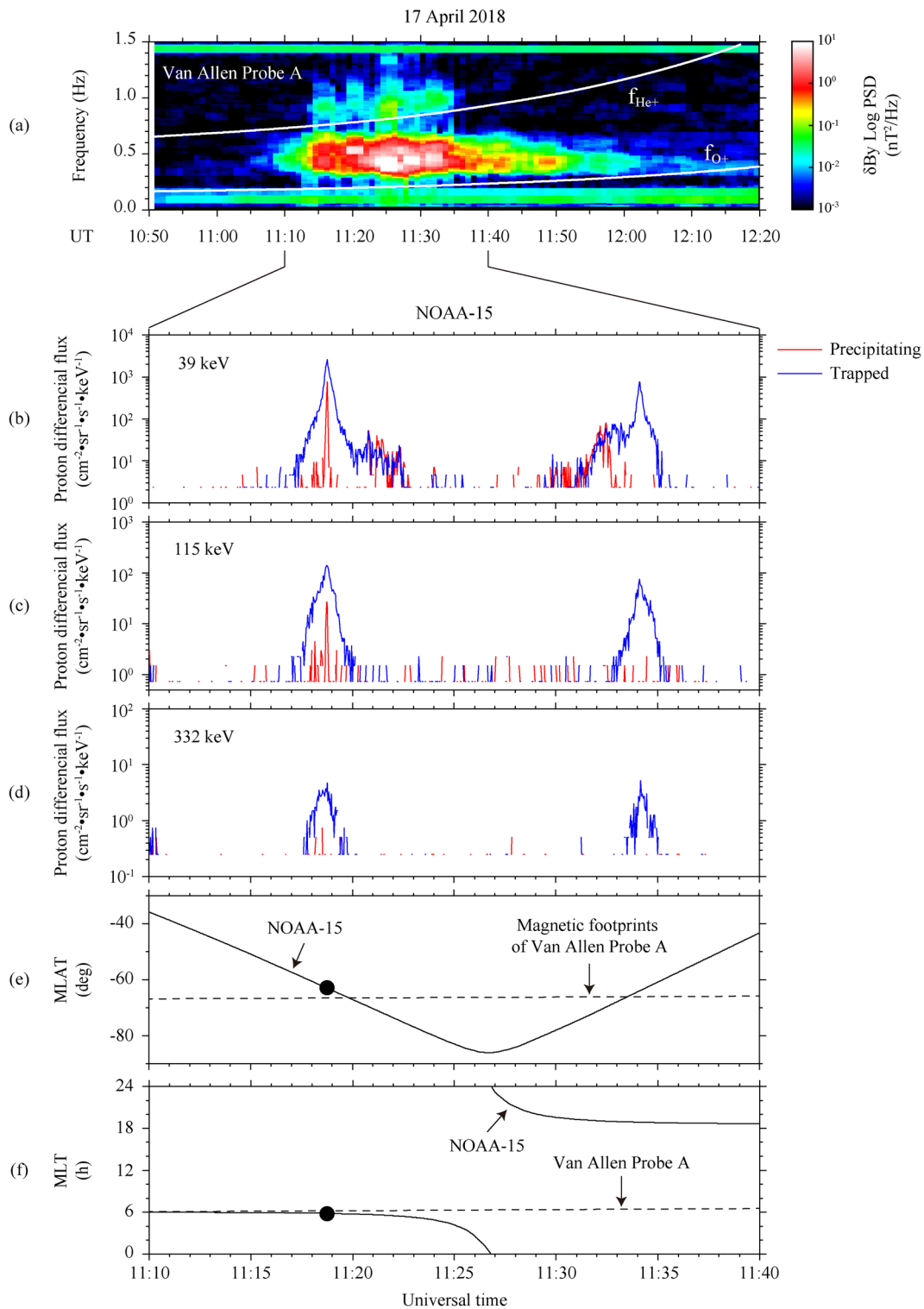


Figure 5. (a) δB_y dynamic spectra at Van Allen Probe A. (b–d) Differential flux for the 39, 115, and 332-keV proton channels of the precipitating (red) and trapped (blue) particles measured by the Medium Energy Proton and Electron Detector (MEPED) instrument onboard NOAA-15 spacecraft. (e) MLAT and (f) MLT of NOAA-15 and Van Allen Probe A. The positions of Van Allen Probe A in MLAT are the magnetic footprints calculated using the Tsyganenko model (1989). MLAT, magnetic latitude; MLT, magnetic local time.

Van Allen Probe A are plotted in Figures 5e and 5f, respectively. The positions of Van Allen Probe A in MLAT are the magnetic footprints calculated using the Tsyganenko model (1989). During the interval of EMIC waves observed just inside the plasmopause near the magnetic equator by Van Allen Probe A (Figure 5a), NOAA-15 spacecraft passed the Southern Hemisphere and observed an isolated peak of the precipitating protons in the differential flux for the 39 and 115 keV proton channels at 11:18:46 UT when the NOAA-15 was located at MLAT = -63.1° and MLT = 5.8 h. The isolated peak region (marked by solid circles in Figures 5e and 5f) is located well equatorward of the isotropic zone, in which the 39-keV trapped and precipitating fluxes are comparable, encountered by NOAA-15 around 11:21 UT as moving higher (auroral) latitudes and close to the projected location (MLAT = -66.5° and MLT = 6.2 h) of Van Allen Probe A with separation of $\Delta\text{MLAT} = \sim 3.4^\circ$ and $\Delta\text{MLT} = \sim 0.4$ h. The small separations in MLAT and MLT indicate that the precipitating energetic protons at NOAA-15 are due to pitch angle scattering associated with EMIC waves at Van Allen Probe A. (e.g., Hyun et al., 2014; K.-H. Kim et al., 2016b; Miyoshi et al., 2008; Yuan et al., 2012; Usanova et al., 2014). The flux ratio of precipitating protons to trapped protons at the isolated peak is 0.29 for the 39-keV channel and 0.19 for the 115-keV channel, indicating that lower energetic protons are scattered more efficiently than higher energetic protons through EMIC waves (Miyoshi et al., 2008).

4. Discussion

Previous observations reported that there is a close correlation between the occurrence of strong EMIC waves and low-energy He⁺ heating. We make a brief comparison of previous and our observations. Young et al. (1981) observed an enhancement of suprathermal He⁺ ions (tens of eV to a few hundred eV) ~ 10 –50 min after the onset of the EMIC waves with frequencies in the vicinity of the He⁺ gyrofrequency at geosynchronous orbit. They showed that EMIC waves are clearly associated with the abundance of cold He⁺ and suggested that the enhancement in He⁺ concentration is a necessary condition to promote EMIC wave growth. Roux et al. (1982) reported that 68% of the geosynchronous EMIC wave events were accompanied by strongly or weakly enhanced He⁺ fluxes in the suprathermal energy range. They also found that cold He⁺ ions can be heated in the direction perpendicular to the background magnetic field up to a few hundred eV when EMIC waves were detected. Anderson and Fuselier (1994) provided clear evidence for a correlation between EMIC waves and perpendicular heated ion distribution by using AMPTE/CCE observations in the outer magnetosphere above geosynchronous orbit and showed that cold He⁺ ions are preferentially and transversely energized to average temperatures of about 35 eV and sometimes above 100 eV through the interaction with EMIC waves. There have been several numerical studies on the preferential heating of cold He⁺ ions by EMIC waves (e.g., Fu et al., 2016; Gendrin & Roux, 1980; Mauk, 1982a, 1982b; Omidi et al., 2010; Omura et al., 1985; Qian et al., 1990).

Unlike previous observations using the data in the outer magnetosphere we report EMIC wave-associated He⁺ heating inside the plasmasphere. Our observations provide a clear correlation between the EMIC wave activity and low-energy (1–10 eV) He⁺ flux enhancement (Figure 3). Comparing the ratio of the helium (J_{He^+}) to proton (J_{H^+}) fluxes integrated over the energy range of 1–10 eV, we confirmed that J_{He^+} is more enhanced than J_{H^+} during EMIC wave activity and that the peaks of the enhanced J_{He^+} appear at the time of the peaks of He-band and H-band wave power without a significant time delay (Figure 4). We also showed that J_{He^+} is mostly enhanced in a direction perpendicular to the magnetic field rather than in a field-aligned direction (Figure 3). These observations indicate that the cold He⁺ ions below 1 eV are preferentially and transversely heated up to 10 eV by the EMIC waves.

To gain more information on pitch angle distribution characteristics of low-energy He⁺ ions during the wave activity, we plot differential He⁺ fluxes from selected energy channels below 10 eV, as a function of time and pitch angle, with the EMIC wave power in Figure 6. The thick white bar in Figure 6d indicates the interval when the He-band wave power is over 10^{-1} nT² (see Figure 3). As noted above, there are strong fluxes during the interval when the H-band and He-band wave powers are enhanced. They occurred over a range of pitch angles from 45° and 120° , representing that the He⁺ flux has asymmetric pitch angle distributions about a pitch angle at 90° . For 1.0 and 1.5-eV He⁺ ions, the flux intensity above 90° pitch angle is larger than that below 90° pitch angle, and there is a flux gap near at 90° pitch angle. This pitch angle distribution is similar to previous observations of X-type He⁺ distributions reported by Anderson and Fuselier (1994),

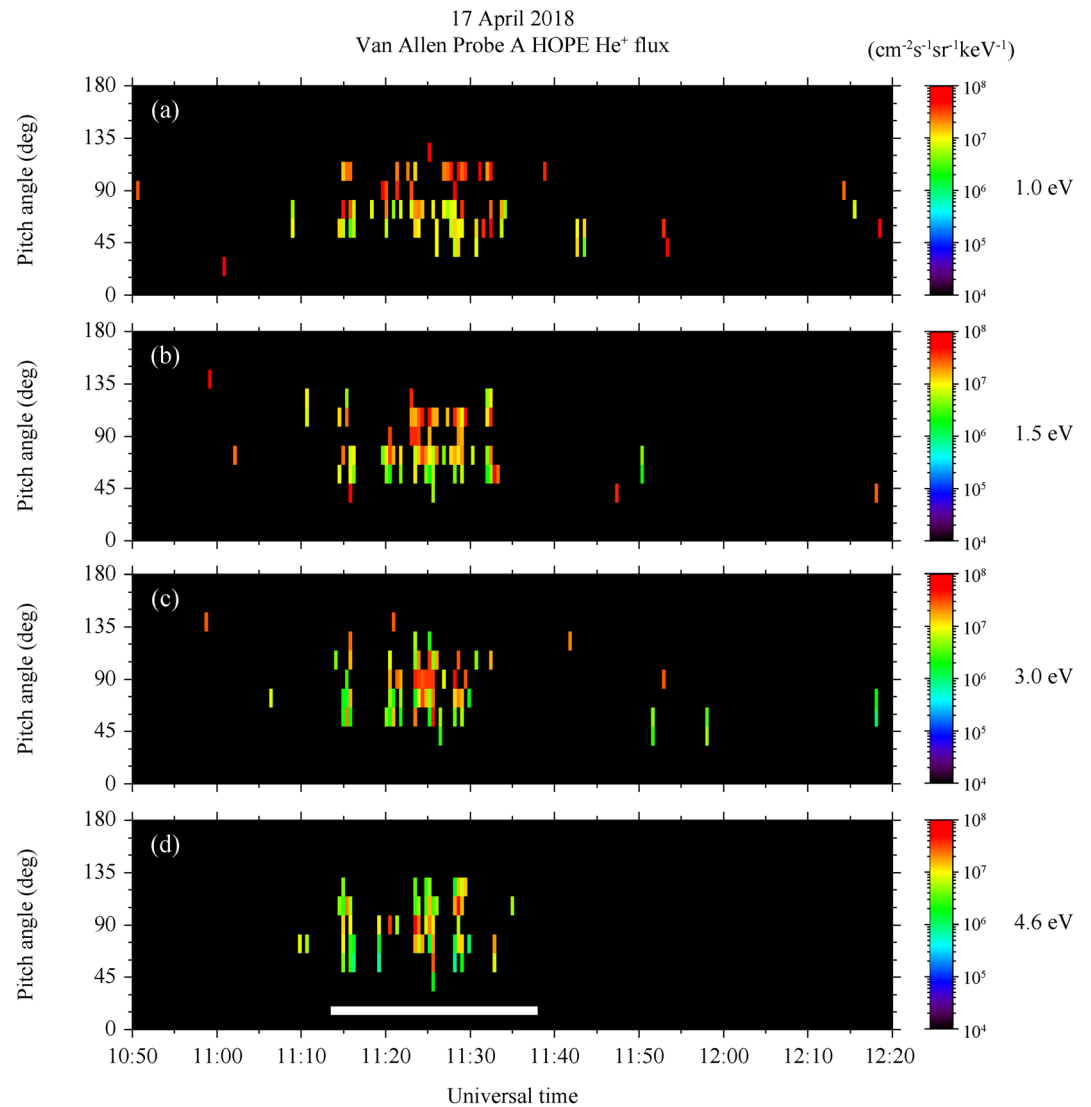


Figure 6. (a–d) Differential He⁺ fluxes from selected energy channels below 10 eV, as a function of time and pitch angle.

who suggested that the X-type distribution is due to a gyroresonant interaction at a point off the magnetic equator where the wave frequency approached the local He⁺ gyrofrequency. However, the 3.0-eV He⁺ ions have strong flux at 90° pitch angle without a gap. Inspection of the selected low-energy He⁺ channels indicates that pitch angle distributions of He⁺ ions heated by EMIC waves show different features at different energy channels.

There are previous theoretical studies of cold He⁺ heating by EMIC waves in the band below or above f_{He^+} (Gendrin & Roux, 1980; Omidi et al., 2010; Omura et al., 1985; Qian et al., 1990). Gendrin and Roux (1980) suggested that He-band waves could energize cold He⁺ ions by gyroresonant interaction ($\Omega_{\text{He}^+} = \omega - kv_{\parallel}$, where k is the wave number and v_{\parallel} is the parallel velocity of the He⁺ ion). Fu et al. (2016) examined the excitation and saturation of EMIC waves using hybrid simulations. In their simulations, cold protons are weakly heated in the direction perpendicular to the background magnetic field when the generated EMIC waves saturate, and cold helium ions have been heated by more than 40 times in the perpendicular direction at the end of the simulation. These simulation results provide that EMIC waves contribute to the high-energy particle scattering and low-energy particle heating. Although Fu et al. (2016) suggest that the low-energy

particle heating is due to the cyclotron resonance at f_{He^+} , they did not discuss which band waves of EMIC waves are more effective contributor to the cold He^+ ion heating.

AMPTE/CCE observations in the outer magnetosphere have shown that low-energy He^+ ion heating occurs more frequently during periods of strong H-band EMIC wave activity rather than He-band wave activity interval (Anderson & Fuselier, 1994). For H-band waves, the gyroresonant heating of cold He^+ ions would occur off the equator because the helium gyrofrequency increases with latitude in the real magnetosphere as the waves generated in the equatorial region propagate toward higher magnetic latitudes. These waves are left-handed from the cutoff frequency up to the crossover frequency and converted into the right-handed mode at the local crossover frequency (Roux et al., 1982; Young et al., 1981). The waves should penetrate the stop band between the cutoff frequency and the helium gyrofrequency to reach the helium gyrofrequency. Thus, they are observed as a right-hand mode near the equatorial region after reflecting at the bi-ion frequency above the helium gyrofrequency (Kim & Johnson, 2016; Roux et al., 1982; Thorne & Horne, 1993). Supporting evidence for the resonant heating of He^+ was provided from the ATS-6 satellite observations at geosynchronous orbit off the magnetic equator (MLAT = $\sim 10^\circ$) (Mauk & McPherron, 1980). The evidence includes that the He^+ ion fluxes are gyrophase bunched by the EMIC wave events for which frequencies normalized to the local proton gyrofrequency were 0.1 (He-band) and 0.33 (H-band), representing that He^+ ions are heated by H-band and/or He-band EMIC waves. The ATS-6 satellite observations provided that the He-band waves were left-handed and the H-band waves were right-handed.

To determine the properties of EMIC waves, which appeared coincidentally with low-energy He^+ flux enhancement, we examine the polarization and ellipticity of transverse magnetic field perturbations δB_x and δB_y during the interval shown in Figure 3, and the results are plotted in Figure 7. We used the method described by Fowler et al. (1967) for the polarization analysis. The degree of polarization (Figure 7c) and ellipticity (Figure 7d) are defined in the two-dimensional spectral matrix constructed from the Fourier transform of the δB_x and δB_y time series. The ellipticity in Figure 7d is shown only for the frequency at which the degree of polarization is higher than 80%. The ellipticity is defined to be negative (positive) if the magnetic field perturbation rotates clockwise (counterclockwise) in the δB_x - δB_y plane, that is, corresponding to left-handed (right-handed) polarization. The degree of polarization is enhanced in the band occupied by the He-band waves, but the high degree of polarization (>80%) is not shown in the entire band. The ellipticity corresponding to the high degree of polarization is mostly below zero, indicating left-handed polarization. The H-band wave does not show the high degree of polarization for the wave activity interval. This observation leads us to conclude that the He-band EMIC waves are the effective contributor to the cold He^+ ion heating.

Young et al. (1981) observed that EMIC waves are clearly associated with the abundance of low-energy (≤ 110 eV) He^+ ions and suggested that the enhanced He^+ concentration promotes EMIC wave growth. To examine whether the enhanced low-energy He^+ ions observed at Van Allen Probe A play some sort of catalytic role in the growth of EMIC waves, we calculate the growth rate of EMIC waves for a plasma composition assumed to be cold protons (89%), cold helium ions (10%), and energetic protons (1%). The energetic proton populations are considered to be $T_\perp/T_\parallel = 2.0$ for two parallel energies of 10 and 33 keV. The observed values of the cold plasma density ($N_e = 165 \text{ cm}^{-3}$) and background magnetic field intensity ($B_T = 210 \text{ nT}$) for the interval of 11:24–11:25 UT at Van Allen Probe A are used for the calculation. It should be noted that 1% energetic protons assumed here is overestimated when the proton fluxes above 10 keV are compared with proton and helium fluxes below 10 eV in the HOPE data (see Figures 2 and 4).

In Figure 8a, the calculated growth rates are plotted against the frequency normalized to f_{H^+} . The magnitude of the peak growth rate in the He-band is significantly greater than that in the H-band for the parallel energy of 33 keV. This is consistent with the observations of strong He-band and weak H-band EMIC waves near the magnetic equator. The calculated frequency is $0.1f_{\text{H}^+}$ at the peak growth rate. As the parallel energy of the energetic protons is reduced to 10 keV, the He-band wave growth rate decreases, and the peak in the growth rate is shifted to higher normalized frequency of $0.14f_{\text{H}^+}$. The peak growth rate of the H-band for 10 keV is comparable to that for 33 keV with a small shift toward higher frequency. It is likely that the growth rate of the H-band wave is hardly affected by parallel energies of energetic protons.

Figure 8b shows the result considering 0.4% warm He^+ ions, 88.6% cold protons, 10% cold helium ions, and 1% energetic protons. B_T , N_e , and the energy and anisotropy factor of the energetic protons are the same as

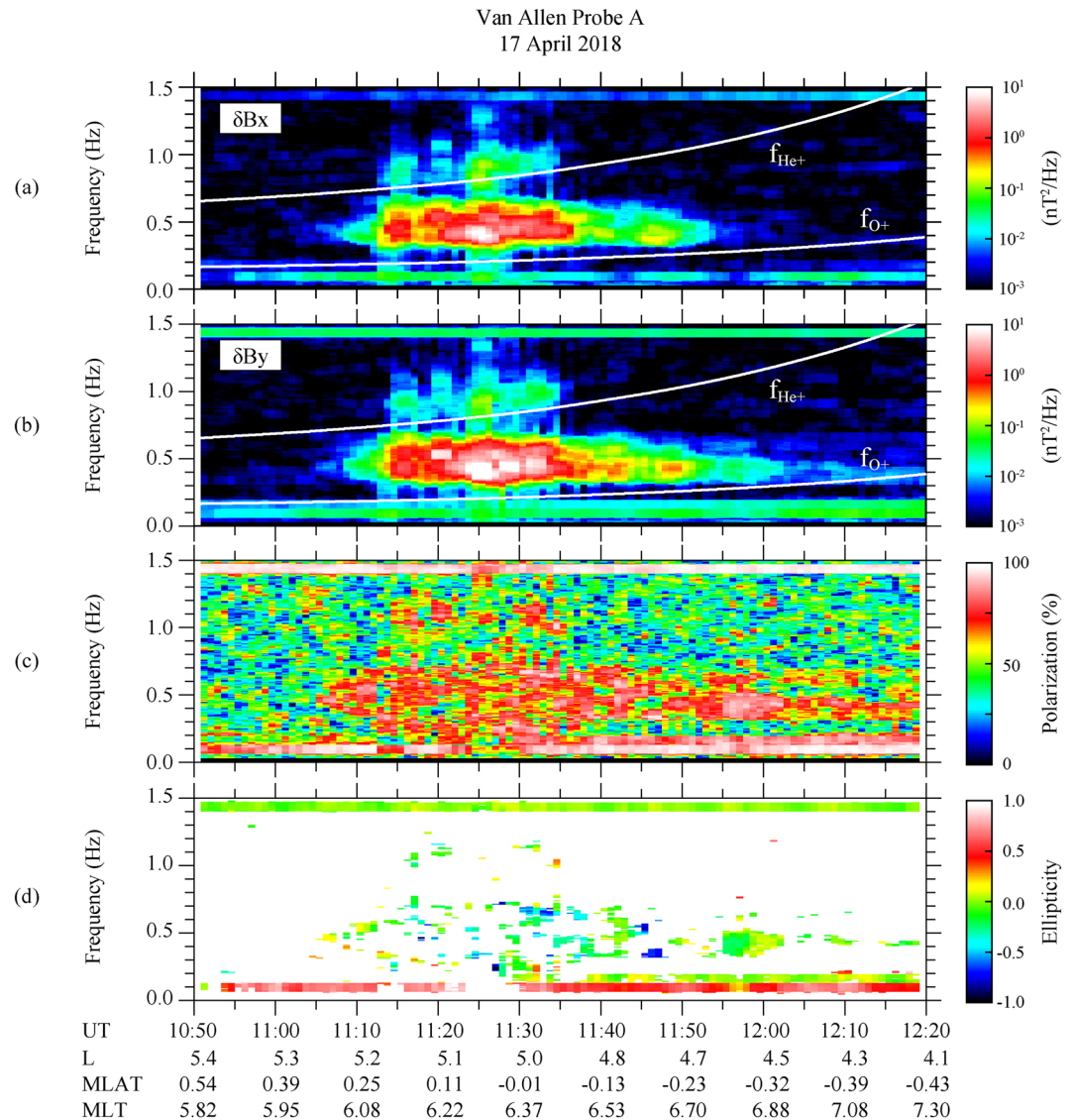


Figure 7. Transverse (a) δB_x and (b) δB_y dynamic spectra. (c) The degree of polarization, and (d) ellipticity defined in the two-dimensional spectral matrix constructed from the δB_x and δB_y time series.

those used to calculate the result shown in Figure 8a. The warm He^+ population consists of the enhanced low-energy He^+ ions at temperatures of 10 eV and 0.7 cm^{-3} observed at Van Allen Probe A. The temperature anisotropy T_{\perp}/T_{\parallel} for the warm He^+ ions is assumed to be 5 because the enhanced He^+ flux is mostly observed in the direction to the background magnetic field. The wave growth rate considering the presence of 0.4% warm He^+ ions is nearly identical to the result calculated with only cold ions and energetic protons, indicating that the low-energy He^+ ions do not promote wave growth. Thus, we suggest that the enhancement of the low-energy He^+ ions (~ 10 eV) is due to preferential heating of cold He^+ (< 1 eV) by EMIC waves (Mauk, 1982a; Qian et al., 1990).

5. Conclusions

Our case study showed a clear correlation between the EMIC wave activity and low-energy He^+ flux enhancement in the direction perpendicular to the ambient magnetic field, providing evidence that cold He^+ ions (< 1 eV) are transversely heated up to 10 eV through the interaction with EMIC waves. The EMIC waves were observed at Van Allen Probe A with a strong spectral intensity in the He-band and weak intensity in

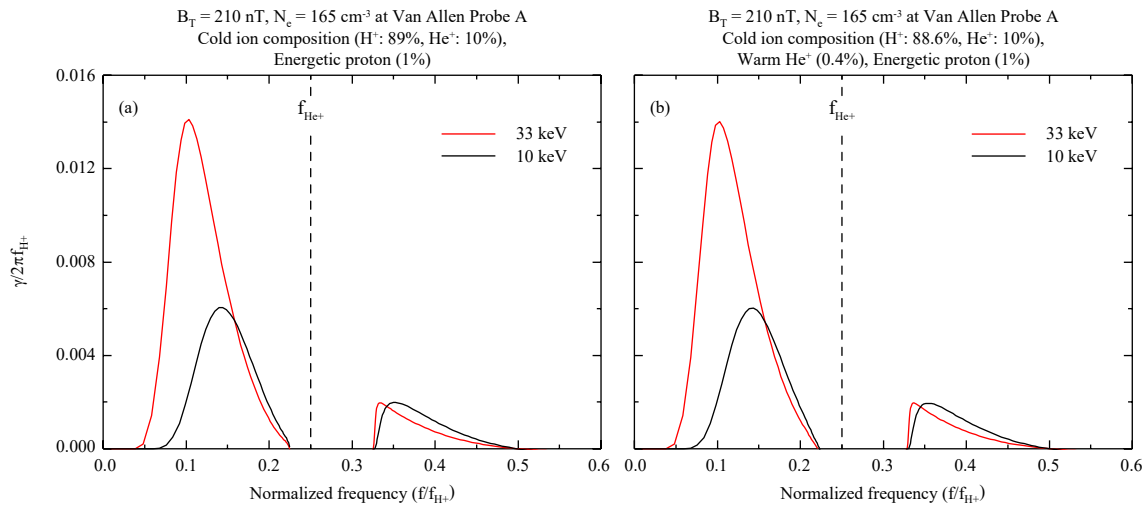


Figure 8. (a) Linear growth rate of EMIC waves as a function of normalized frequency at Van Allen Probe A orbit for a plasma composition assumed to be cold protons (89%), cold helium ions (10%), and energetic protons (1%). The energetic proton populations are considered to be $T_{\perp}/T_{\parallel} = 2.0$ for two parallel energies of 10 keV (black) and 33 keV (red). The cold plasma density ($N_e = 165 \text{ cm}^{-3}$) and background magnetic field intensity ($B_T = 210 \text{ nT}$) observed at Van Allen Probe A for the interval of 11:24–11:25 UT are used for the calculation. (b) The same as the magnetic field intensity and plasma parameters used to calculate the result shown in Figure 10a except for 0.4% warm He^+ ions, 88.6% cold protons. EMIC, electromagnetic ion cyclotron.

the H-band when the spacecraft was just inside the plasmopause near the magnetic equator. Previous theoretical studies suggested that cold He^+ ions can be heated by H-band and/or He-band EMIC waves. In our case it is likely that He-band waves play a key role in heating the cold He^+ ions.

The case event in our study shows that the He^+ ions heated up to 10 eV. This energy is lower than that in the previous studies. Since the present study is based on only one event observed on a single Van Allen Probe A pass inside the plasmasphere, we cannot generalize the quantitative argument for the question: What is a critical factor for the EMIC wave-driven He^+ heating? To answer the question, we need to observe the EMIC wave-associated He^+ heating events at various latitudes, longitudes, and radial distances and under various background plasma and magnetic field conditions. Currently, we statistically examine the relationship between EMIC He-band waves and cold ion heating, and the results will be presented in a related publication.

Data Availability Statement

The Van Allen Probe A EMFISIS data were obtained from the University of Iowa (<http://emfisis.physics.uiowa.edu>), and the Van Allen Probe A HOPE data were obtained from the Van Allen Probes ECT website (<https://www.rbsp-ect.lanl.gov/science/DataDirectories.php/>). NOAA-15 data are available at <https://cdaweb.gsfc.nasa.gov>.

Acknowledgments

The work of K.-H. Kim was supported by the Basic Science Research Program through NRF funded by NRF-2019R1F1A105444 and also supported by project PE21020 of the Korea Polar Research Institute. The work of H.-J. Kwon was supported by the Basic Science Research Program through NRF funded by NRF-2020R1C1C1003640.

References

- Allen, R. C., Zhang, J.-C., Kistler, L. M., Spence, H. E., Lin, R.-L., Klecker, B., et al. (2015). A statistical study of EMIC waves observed by Cluster: 1. Wave properties. *Journal of Geophysical Research: Space Physics*, *120*, 5574–5592. <https://doi.org/10.1002/2015JA021333>
- Anderson, B. J., Erlandson, R. E., & Zanetti, L. J., (1992a). A statistical study of Pc 1–2 magnetic pulsations in the equatorial magnetosphere: 1. Equatorial occurrence distributions. *Journal of Geophysical Research*, *97*(A3), 3075–3088.
- Anderson, B. J., Erlandson, R. E., & Zanetti, L. J., (1992b). A statistical study of Pc 1–2 magnetic pulsations in the equatorial magnetosphere: 2. Wave properties. *Journal of Geophysical Research*, *97*(A3), 3089–3101.
- Anderson, B. J., & Fuselier, S. A. (1994). Response of thermal ions to electromagnetic ion cyclotron waves. *Journal of Geophysical Research*, *99*(A10), 19413–19425.
- Bingley, L., Angelopoulos, V., Sibeck, D., Zhang, X., & Halford, A. (2019). The evolution of a pitch-angle “bite-out” scattering signature caused by EMIC wave activity: A case study. *Journal of Geophysical Research: Space Physics*, *124*, 5042–5055. <https://doi.org/10.1029/2018JA026292>
- Bortnik, J., Cutler, J. W., Dunson, C., Bleier, T. E., & McPherron, R. L. (2008). Characteristics of low-latitude Pc1 pulsations during geomagnetic storms. *Journal of Geophysical Research*, *113*, A04201. <https://doi.org/10.1029/2007JA012867>
- Carpenter, D. L., & Anderson, R. R. (1992). An ISEE/whistler model of equatorial electron density in the magnetosphere. *Journal of Geophysical Research*, *97*(A2), 1097–1108.

- Chen, M. W., Roeder, J. L., Fennell, J. F., Lyons, L. R., & Schulz, M. (1998). Simulations of ring current proton pitch angle distributions. *Journal of Geophysical Research*, *103*(A1), 165–178.
- Clilverd, M. A., Rodger, C. J., Millan, R. M., Sample, J. G., Kokorowski, M., McCarthy, M. P., et al. (2007). Energetic particle precipitation into the middle atmosphere triggered by a coronal mass ejection. *Journal of Geophysical Research*, *112*, A12206. <https://doi.org/10.1029/2007JA012395>
- Cornwall, J. M. (1965). Cyclotron instabilities and electromagnetic emission in the ultra low frequency and very low frequency ranges. *Journal of Geophysical Research*, *70*(1), 61–69.
- Engebretson, M. J., Peterson, W. K., Posch, J. L., Klatt, M. R., Anderson, B. J., Russell, C. T., et al. (2002). Observations of two types of Pc 1–2 pulsations in the outer dayside magnetosphere. *Journal of Geophysical Research*, *107*(A12), 1451. <https://doi.org/10.1029/2001JA000198>
- Engebretson, M. J., Posch, J. L., Wygant, J. R., Kletzing, C. A., Lessard, M. R., Huang, C.-L., et al. (2015). Van Allen probes, NOAA, GOES, and ground observations of an intense EMIC wave event extending over 12 h in magnetic local time. *Journal of Geophysical Research: Space Physics*, *120*, 5465–5488. <https://doi.org/10.1002/2015JA021227>
- Evans, D. S., & Greer, M. S. (2004). *Polar orbiting environmental satellite space environment monitor-2: Instrument descriptions and archive data documentation* (NOAA Tech. Memo. 1.4). Boulder, CO: Space Environment Laboratory.
- Ferradas, C. P., Zhang, J. C., Spence, H. E., Kistler, L. M., Larsen, B. A., Reeves, G., et al. (2016). Ion nose spectral structures observed by the Van Allen Probes. *Journal of Geophysical Research: Space Physics*, *121*, 12025–12046. <https://doi.org/10.1002/2016JA022942>
- Fowler, R. A., Kotick, B. J., & Elliott, R. D. (1967). Polarization analysis of natural and artificially induced geomagnetic micropulsations. *Journal of Geophysical Research*, *72*(11), 2871–2883.
- Fraser, B. J., & McPherron, R. L. (1982). Pc 1–2 magnetic pulsation spectra and heavy ion effects at synchronous orbit: ATS 6 results. *Journal of Geophysical Research*, *87*(A6), 4560–4566.
- Fraser, B. J., & Nguyen, T. S. (2001). Is the plasmapause a preferred source region of electromagnetic ion cyclotron waves in the magnetosphere?. *Journal of Atmospheric and Solar-Terrestrial Physics*, *63*, 1225–1247.
- Fraser, B. J., Samson, J. C., Hu, Y. D., McPherron, R. L., & Russell, C. T. (1980). Electromagnetic ion cyclotron waves observed near the oxygen cyclotron frequency by ISEE 1 and 2. *Journal of Geophysical Research*, *97*(A3), 3063–3074.
- Fu, X., Cowee, M. M., Jordanova, V. K., Gary, S. P., Reeves, G. D., & Winske, D. (2016). Predicting electromagnetic ion cyclotron wave amplitude from unstable ring current plasma conditions. *Journal of Geophysical Research: Space Physics*, *121*, 10954–10965. <https://doi.org/10.1002/2016JA023303>
- Funsten, H. O., Skoug, R. M., Guthrie, A. A., MacDonald, E. A., Baldonado, J. R., Harper, R. W., et al. (2013). Helium, oxygen, proton, and electron (HOPE) mass spectrometer for the Radiation Belt Storm Probes mission. *Space Science Reviews*, *179*(1–4), 423–484. <https://doi.org/10.1007/s11214-013-9968-7>
- Gendrin, R., & Roux, A. (1980). Energization of helium ions by proton induced hydromagnetic waves. *Journal of Geophysical Research*, *85*(A9), 4577–4586.
- Goldstein, J. S., Pascuale, S. D., Kletzing, C., Kurth, W., Genestreti, K. J., Skoug, R. M., et al. (2014). Simulation of Van Allen Probes plasmapause encounters. *Journal of Geophysical Research: Space Physics*, *119*, 7464–7484. <https://doi.org/10.1002/2014JA020252>
- Hendry, A. T., Rodger, C. J., Clilverd, M. A., Engebretson, M. J., Mann, I. R., Lessard, M. R., et al. (2016). Confirmation of EMIC wave-driven relativistic electron precipitation. *Journal of Geophysical Research: Space Physics*, *121*, 5366–5383. <https://doi.org/10.1002/2015JA022224>
- Hyun, K., Kim, K.-H., Lee, E., Kwon, H.-J., Lee, D.-H., & Jin, H. (2014). Loss of geosynchronous relativistic electrons by EMIC wave scattering under quiet geomagnetic conditions. *Journal of Geophysical Research: Space Physics*, *119*, 8357–8371. <https://doi.org/10.1002/2014JA020234>
- Ishida, J., Kokubun, S., & McPherron, R. L. (1987). Substorm effects on spectral structures of Pc 1 waves at synchronous orbit. *Journal of Geophysical Research*, *92*(A1), 143–158.
- Keika, K., Takahashi, K., Ukhorskiy, A. Y., & Miyoshi, Y. (2013). Global characteristics of electromagnetic ion cyclotron waves: Occurrence rate and its storm dependence. *Journal of Geophysical Research: Space Physics*, *118*, 4135–4150. <https://doi.org/10.1002/jgra.50385>
- Kennel, C. F., & Petschek, H. E. (1966). Limit on stably trapped particle fluxes. *Journal of Geophysical Research*, *71*(1), 1–28.
- Kim, E.-H., & Johnson, J. R. (2016). Full-wave modeling of EMIC waves near the He⁺ gyrofrequency. *Geophysical Research Letters*, *43*, 13–21. <https://doi.org/10.1002/2015GL066978>
- Kim, G.-J., Kim, K.-H., Lee, D.-H., Kwon, H.-J., & Park, J.-S. (2016). Occurrence of EMIC waves and plasmaspheric plasmas derived from THEMIS observations in the outer magnetosphere: Revisit. *Journal of Geophysical Research: Space Physics*, *121*, 9443–9458. <https://doi.org/10.1002/2016JA023108>
- Kim, H., Clauer, C. R., Gerrard, A. J., Engebretson, M. J., Hartinger, M. D., Lessard, M. R., et al. (2017). Conjugate observations of electromagnetic ion cyclotron waves associated with traveling convection vortex events. *Journal of Geophysical Research: Space Physics*, *122*, 7336–7352. <https://doi.org/10.1002/2017JA024108>
- Kim, K.-H., Omura, Y., Jin, H., & Hwang, J. (2017). A case study of EMIC waves associated with sudden geosynchronous magnetic field changes. *Journal of Geophysical Research: Space Physics*, *122*, 3322–3341. <https://doi.org/10.1002/2016JA023391>
- Kim, K.-H., Park, J.-S., Omura, Y., Shiokawa, K., Lee, D.-H., Kim, G.-J., et al. (2016a). Spectral characteristics of steady quiet-time EMIC waves observed at geosynchronous orbit. *Journal of Geophysical Research: Space Physics*, *121*, 8640–8660. <https://doi.org/10.1002/2016JA022957>
- Kim, K.-H., Shiokawa, K., Mann, I. R., Park, J.-S., Kwon, H.-J., Hyun, K., & Connors, M. (2016b). Longitudinal frequency variation of long-lasting EMIC Pc1–Pc2 waves localized in the inner magnetosphere. *Geophysical Research Letters*, *43*, 1039–1046. <https://doi.org/10.1002/2015GL067536>
- Kletzing, C. A., Kurth, W. S., Acuna, M., MacDowall, R. J., Torbert, R. B., Averkamp, T., et al. (2013). The electric and magnetic field instrument suite and integrated science (EMFISIS) on RBSP. *Space Science Reviews*, *179*(1–4), 127–181. <https://doi.org/10.1007/s11214-013-9993-6>
- Kozyra, J. U., Cravens, T. E., Nagy, A. F., Fontheim, E. G., & Ong, R. S. B. (1984). Effects of energetic heavy ions on electromagnetic ion cyclotron wave generation in the plasmapause region. *Journal of Geophysical Research*, *89*(A4), 2217–2233.
- Kurth, W. S., De Pascuale, S., Faden, J. B., Kletzing, C. A., Hospodarsky, G. B., Thaller, S., & Wygant, J. R. (2015). Electron densities inferred from plasma wave spectra obtained by the Waves instrument on Van Allen Probes. *Journal of Geophysical Research: Space Physics*, *120*, 904–914. <https://doi.org/10.1002/2014JA020857>
- Kwon, H. J., Kim, K. H., Jee, G., Park, J. S., Jin, H., & Nishimura, Y. (2015). Plasmapause location under quiet geomagnetic conditions ($K_p \leq 1$): THEMIS observations. *Geophysical Research Letters*, *42*, 7303–7310. <https://doi.org/10.1002/2015GL066090>
- Kwon, J.-W., Kim, K.-H., Jin, H., Kwon, H.-J., Jee, G., Shiokawa, K., & Connors, M. (2020). Statistical study of EMIC Pc1–Pc2 waves observed at subauroral latitudes. *Journal of Atmospheric and Solar-Terrestrial Physics*, *205*, 105292. <https://doi.org/10.1016/j.jastp.2020.105292>

- Liu, S., Zhang, J., Chen, L., Zhu, H., & He, Z. (2018). Examining wave vector and minimum cyclotron resonant electron energy of EMIC waves with Magnetospheric Multiscale mission. *Geophysical Research Letters*, *45*, 10138–10149. <https://doi.org/10.1029/2018GL079737>
- Lyons, L. R., & Thorne, R. M. (1972). Parasitic pitch angle diffusion of radiation belt particles by ions cyclotron waves. *Journal of Geophysical Research*, *77*(28), 5608–5617.
- Mann, I. R., Usanova, M. E., Murphy, K., Robertson, M. T., Milling, D. K., Kale, A., & Raita, T. (2014). Spatial localization and ducting of EMIC waves: Van Allen Probes and groundbased observations. *Geophysical Research Letters*, *41*, 785–792. <https://doi.org/10.1002/2013GL058581>
- Mauk, B. H., McIlwain, C. E., & McPherron, R. L. (1981). Helium cyclotron resonance within the Earth's magnetosphere. *Geophysical Research Letters*, *8*, 103–106. <https://doi.org/10.1029/GL008i001p00103>
- Mauk, B. H., & McPherron, R. L. (1980). An experimental test of the electromagnetic ion cyclotron instability within the Earth's magnetosphere. *The Physics of Fluids*, *23*, 2111. <https://doi.org/10.1063/1.862873>
- Mauk, B. H. (1982a). Helium resonance and dispersion effects on geostationary Alfvén/ion cyclotron waves. *Journal of Geophysical Research*, *87*(A11), 9107–9119.
- Mauk, B. H. (1982b). Electromagnetic wave energization of heavy ions by the electric 'phase bunching' process. *Geophysical Research Letters*, *9*(10), 1163–1166.
- Meredith, N. P., Thorne, R. M., Horne, R. B., Summers, D., Fraser, B. J., & Anderson, R. R. (2003). Statistical analysis of relativistic electron energies for cyclotron resonance with EMIC waves observed on CRRES. *Journal of Geophysical Research*, *108*(A6), 1250. <https://doi.org/10.1029/2002JA009700>
- Min, K., Lee, J., Keika, K., & Li, W. (2012). Global distribution of EMIC waves derived from THEMIS observations. *Journal of Geophysical Research*, *117*, A05219. <https://doi.org/10.1029/2012JA017515>
- Miyoshi, Y., Sakaguchi, K., Shiokawa, K., Evans, D., Albert, J., Connors, M., & Jordanova, V. (2008). Precipitation of radiation belt electrons by EMIC waves, observed from ground and space. *Geophysical Research Letters*, *35*, L23101. <https://doi.org/10.1029/2008GL035727>
- Nomura, R., Shiokawa, K., Pilipenko, V., & Shevtsov, B. (2011). Frequency-dependent polarization characteristics of Pc1 geomagnetic pulsations observed by multipoint ground stations at low latitudes. *Journal of Geophysical Research*, *116*, A01204. <https://doi.org/10.1029/2010JA015684>
- Olson, J. V., & Lee, L. C. (1983). Pc1 wave generation by sudden impulses. *Planetary and Space Science*, *31*(3), 295–302. [https://doi.org/10.1016/0032-0633\(83\)90079-X](https://doi.org/10.1016/0032-0633(83)90079-X)
- Omidi, N., Thorne, R. M., & Bortnik, J. (2010). Nonlinear evolution of EMIC waves in a uniform magnetic field: 1. Hybrid simulations. *Journal of Geophysical Research*, *115*, A12241. <https://doi.org/10.1029/2010JA015607>
- Omura, Y., Ashourabdalla, M., Gendrin, R., & Quest, K. (1985). Heating of thermal helium in the equatorial magnetosphere: A simulation study. *Journal of Geophysical Research*, *90*(A9), 8281–8292.
- Park, J.-S., Kim, K.-H., Shiokawa, K., Lee, D.-H., Lee, E., Kwon, H.-J., et al. (2016). EMIC waves observed at geosynchronous orbit under quiet geomagnetic conditions ($K_p \leq 1$). *Journal of Geophysical Research: Space Physics*, *121*, 1377–1390. <https://doi.org/10.1002/2015JA021968>
- Qian, S., Hudsona, M. K., & Roth, I. (1990). Particle simulation of ion heating in the ring current. *Journal of Geophysical Research*, *95*(A2), 1001–1013.
- Rodger, C. J., Raita, T., Clilverd, M. A., Seppälä, A., Dietrich, S., Thomsen, N. R., & Ulich, T. (2008). Observations of relativistic electron precipitation from the radiation belts driven by EMIC waves. *Geophysical Research Letters*, *35*, L16106. <https://doi.org/10.1029/2008GL034804>
- Roux, A., Perraut, S., Rauch, J. L., de Villedary, C., Kremser, G., Korth, A., & Young, D. T. (1982). Wave-particle interactions near ω_{He^+} observed on board GEOS 1 and 2: 2. Generation of ion cyclotron waves and heating of He^+ ions. *Journal of Geophysical Research*, *87*(A10), 8174–8190.
- Saikin, A. A., Zhang, J.-C., Allen, R. C., Smith, C. W., Kistler, L. M., Spence, H. E., & Jordanova, V. K. (2015). The occurrence and wave properties of H^+ , He^+ , and O^+ -band EMIC waves observed by the Van Allen Probes. *Journal of Geophysical Research: Space Physics*, *120*, 7477–7492. <https://doi.org/10.1002/2015JA021358>
- Sakaguchi, K., Kasahara, Y., Shoji, M., Omura, Y., Miyoshi, Y., Nagatsuma, T., et al. (2013). Akebono observations of EMIC waves in the slot region of the radiation belts. *Geophysical Research Letters*, *40*, 5587–5591. <https://doi.org/10.1002/2013GL058258>
- Sakaguchi, K., Shiokawa, K., Miyoshi, Y., Otsuka, Y., Ogawa, T., Asamura, K., & Connors, M. (2008). Simultaneous appearance of isolated auroral arcs and Pc 1 geomagnetic pulsations at subauroral latitudes. *Journal of Geophysical Research*, *113*, A05201. <https://doi.org/10.1029/2007JA012888>
- Sandanger, M. I., Soraas, F., Sørbo, M., Aarsnes, K., Oksavik, K., & Evans, D. S. (2009). Relativistic electron losses related to EMIC waves during CIR and CME storms. *Journal of Atmospheric and Solar-Terrestrial Physics*, *71*, 1126–1144. <https://doi.org/10.1016/j.jastp.2008.07.006>
- Sarno-Smith, L. K., Liemohn, M. W., Katus, R. M., Skoug, R. M., Larsen, B. A., Thomsen, M. F., et al. (2015). Postmidnight depletion of the high-energy tail of the quiet plasmasphere. *Journal of Geophysical Research: Space Physics*, *120*, 1646–1660. <https://doi.org/10.1002/2014JA020682>
- Summers, D., & Thorne, R. M. (2003). Relativistic electron pitch angle scattering by electromagnetic ion cyclotron waves during geomagnetic storms. *Journal of Geophysical Research*, *108*(A4), 1143. <https://doi.org/10.1029/2002JA009489>
- Thorne, R. M., & Horne, R. B. (1993). Cyclotron absorption of ion-cyclotron waves at the bi-ion frequency. *Geophysical Research Letters*, *20*(4), 317–320.
- Thorne, R. M., & Kennel, C. F. (1971). Relativistic electron precipitation during magnetic storm main phase. *Journal of Geophysical Research*, *76*(19), 4446–4453.
- Tsyganenko, N. A. (1989). A magnetospheric magnetic field model with a warped tail current sheet. *Planetary and Space Science*, *37*, 5–20.
- Tsyganenko, N. A., & Sitnov, M. I. (2005). Modeling the dynamics of the inner magnetosphere during strong geomagnetic storms. *Journal of Geophysical Research*, *110*, A03208. <https://doi.org/10.1029/2004JA010798>
- Usanova, M. E., Drozdov, A., Orlova, K., Mann, I. R., Shprits, Y., Robertson, M. T., et al. (2014). Effect of EMIC waves on relativistic and ultrarelativistic electron populations: Ground-based and Van Allen Probes observations. *Geophysical Research Letters*, *41*, 1375–1381. <https://doi.org/10.1002/2013GL059024>
- Usanova, M. E., Mann, I. R., Bortnik, J., Shao, L., & Angelopoulos, V. (2012). THEMIS observations of electromagnetic ion cyclotron wave occurrence: Dependence on AE, SYMH, and solar wind dynamic pressure. *Journal of Geophysical Research*, *117*, A10218. <https://doi.org/10.1029/2012JA018049>
- Usanova, M. E., Mann, I. R., Rae, I. J., Kale, Z. C., Angelopoulos, V., Bonnell, J. W., et al. (2008). Multipoint observations of magnetospheric compression-related EMIC Pc1 waves by THEMIS and CARISMA. *Geophysical Research Letters*, *35*, L17S25. <https://doi.org/10.1029/2008GL034458>

- Young, D. T., Perraut, S., Roux, A., de Villedary, C., Gendrin, R., Korth, A., et al. (1981). Wave-particle interactions near ω_{He^+} observed on GEOS 1 and 2. Propagation of ion cyclotron waves in He⁺-rich plasma. *Journal of Geophysical Research*, *86*(A8), 6755–6772.
- Yuan, Z., Xiong, Y., Wang, D., Li, M., Deng, X., Yahnin, A. G., et al. (2012). Characteristics of precipitating energetic ions/electrons associated with the wave-particle interaction in the plasmaspheric plume. *Journal of Geophysical Research*, *117*, A08324. <https://doi.org/10.1029/2012JA017783>
- Yuan, Z., Yu, X., Wang, D., Huang, S., Li, H., Yu, T., et al. (2016). In situ evidence of the modification of the parallel propagation of EMIC waves by heated He⁺ ions. *Journal of Geophysical Research: Space Physics*, *121*, 6711–6717. <https://doi.org/10.1002/2016JA022573>
- Zhang, J.-C., Kistler, L. M., Mouikis, C. G., Klecker, B., Sauvaud, J.-A., & Dunlop, M. W. (2011). A statistical study of EMIC wave-associated He⁺ energization in the outer magnetosphere: Cluster/CODIF observations. *Journal of Geophysical Research*, *116*, A11201. <https://doi.org/10.1029/2011JA016690>
- Zhang, X.-J., Li, W., Ma, Q., Thorne, R. M., Angelopoulos, V., Bortnik, J., et al. (2016). Direct evidence for EMIC wave scattering of relativistic electrons in space. *Journal of Geophysical Research: Space Physics*, *121*, 6620–6631. <https://doi.org/10.1002/2016JA022521>